



Targeted metabolomics in cultured cells and tissues by mass spectrometry: Method development and validation



Anas M. Abdel Rahman^{a,b}, Judy Pawling^a, Michael Ryczko^{a,c}, Amy A. Caudy^{c,e}, James W. Dennis^{a,b,c,d,*}

^a Lunenfeld-Tanenbaum Research Institute, Mount Sinai Hospital, 600 University Avenue R988, Toronto, Ontario M5G 1X5, Canada

^b Faculty of Pharmacy, Yarmouk University, Irbid, Jordan

^c Department of Molecular Genetics, University of Toronto, Canada

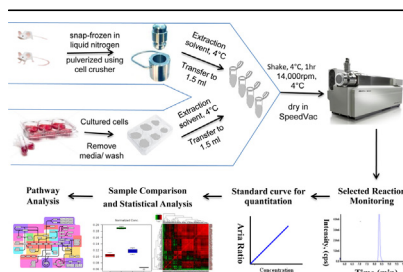
^d Department of Laboratory Medicine and Pathology, University of Toronto, Canada

^e The Donnelly Centre, University of Toronto, Canada

HIGHLIGHTS

- This study introduces a valid bioanalytical method for metabolic profiling.
- The method validation and stability were studied carefully based on USFDA guidelines.
- The targeted metabolomics method was tested on couple of biological systems cell lines and mouse tissue.

GRAPHICAL ABSTRACT



ARTICLE INFO

Article history:

Received 19 April 2014

Received in revised form 5 June 2014

Accepted 9 June 2014

Available online 12 June 2014

Keywords:

Metabolism
Mass spectrometry
Sensitivity
Precision
Diagnostics

ABSTRACT

Metabolomics is the identification and quantitation of small bio-molecules (metabolites) in biological samples under various environmental and genetic conditions. Mass spectrometry provides the unique opportunity for targeted identification and quantification of known metabolites by selective reaction monitoring (SRM). However, reproducibility of this approach depends on careful consideration of sample preparation, chemical classes, and stability of metabolites to be evaluated. Herein, we introduce and validate a targeted metabolite profiling workflow for cultured cells and tissues by liquid chromatography–triple quadrupole tandem mass spectrometry. The method requires a one-step extraction of water-soluble metabolites and targeted analysis of central metabolites that include glycolysis, amino acids, nucleotides, citric acid cycle, and the hexosamine biosynthetic pathway. The sensitivity, reproducibility and molecular stability of each targeted metabolite were assessed under experimental conditions. Quantitation of metabolites by peak area ratio was linear with a dilution over a 4 fold dynamic range with minimal deviation $R^2=0.98$. Inter- and intra-day precision with cells and tissues had an average coefficient of variation <15% for cultured cell lines, and somewhat higher for mouse liver tissues. The method applied in triplicate measurements readily distinguished immortalized cells from malignant cells, as well as mouse littermates based on their hepatic metabolic profiles.

© 2014 Elsevier B.V. All rights reserved.

1. Introduction

Cells control the import of nutrients and their conversion into macromolecules and energy through a network of enzymatic reactions referred to as central metabolism. Nutrient flux into

* Corresponding author at: Mount Sinai Hospital, Lunenfeld-Tanenbaum Research Institute, 600 University Ave. Room#988, Toronto, Canada.
Tel.: +1 416 586 4800/8233; fax: +1 416 586 8587.

E-mail address: dennis@lunenfeld.ca (J.W. Dennis).

oxidative respiration and biosynthesis of macromolecules depends on tissue type, extracellular cues, genetic variation, age and disease. Measuring the steady state levels and turnover rates of metabolites in cells and tissues can provide molecular profiles of health, diseases, and heritable conditions [1]. Most metabolites are pathway intermediates, thus metabolic profiles comparing conditions such as transformed versus normal cells can predict changes in substrate–product flux, and thereby possible changes in specific enzyme activities [2]. The metabolic profiles provide unique information that when used together with genome-wide analysis such as gene expression can reveal molecular mechanism [3,4]. Reprogramming of metabolism in cancer cells is often described as the Warburg effect [5], and involves increased glucose uptake and flux into anabolic pathway needed for cell growth [6,7]. Cancer metabolism has features that can be detected by metabolic profiles, and certain features point to vulnerabilities that could be targeted by new cancer therapies [8,9].

Glycolytic metabolites are directed away from the tricarboxylic acid (TCA) cycle and oxidative respiration, and into the biosynthesis of lipids, nucleic acids, and proteins [10–12]. Glutamine uptake is also increased, and converted to glutamate and α -ketoglutarate (α -KG), an anaplerotic substrate that supports the TCA cycle [7,8]. Glutamine is also a nitrogen donor for synthesis of purines, pyrimidines, and nonessential amino acids. The malate and citrate produced in the TCA cycle are exported from the mitochondria, and converted to pyruvate and α -KG, respectively, plus NADPH, which contributes to fatty acid synthesis and suppresses reactive oxygen species. Cell division requires both anabolic substrates and large amounts of ATP that only oxidative respiration can deliver. Thus, glutamine is a major contributor to both anabolic pathways and oxidative respiration [6,7].

The metabolome includes a wide spectrum of small molecules that vary in their chemical and physical properties such as polarity, hydrophobicity and solubility [13,14,19]. This molecular diversity is the main challenge in achieving quantitative analytical chemistry in a single method with minimal technical variations [15,16,20]. Metabolic profiling on cells (the metabolic fingerprint) and on the cell growth medium (the metabolic footprint) are the complementary approaches to study pathway(s) and inter-conversion of compounds such as amino acids or carbohydrates [11]. Combining

metabolic profiling and molecular genetics has become a powerful approach to study cancer development and progression, with potential for better diagnosis and prognosis [2,3,17,18].

Metabolite profiling requires a sophisticated strategy to rapidly extract and preserve metabolites, to identify the chemical structures with high confidence, and to quantify them with high accuracy. The metabolome includes a wide spectrum of small molecules that vary in their chemical and physical properties such as polarity, hydrophobicity and solubility [13,19]. Molecular diversity of the metabolites is a major challenge in achieving quantitative analytical chemistry in a single method with minimal technical variations [15,20]. Herein, we report validation for a method of metabolite extraction from cells and tissue extracts, and targeted analysis by liquid chromatography–tandem mass spectrometry (LC–MS/MS) (Fig. 1) [21]. The sensitivity, selectivity and linearity of LC–MS/MS data were evaluated, as well as the stability of the measured metabolites under defined preparation and analysis conditions [22–24]. The experimental variation in extracted metabolites was determined within and between three independent experiments. Comparison of a transformed and two immortalized cell lines revealed multiple known features of metabolic reprogramming observed in cancer cells.

2. Materials and methods

2.1. Chemicals and reagents

Metabolite standards and reagents were obtained from Sigma Chemicals (St. Louis, MO) at a minimal purity of 98%. Isotope labeled internal standards, D_7 -glucose and $^{13}C_9$ ^{15}N -tyrosine, were purchased from Cambridge Isotope, Inc. (Woburn, MA). All organic solvents and water used in sample and mobile phase preparation were HPLC grade and obtained from Fisher Scientific (Fair Lawn, NJ).

2.2. Stock and working standard solution

A standard solution at a concentration of 10 μ M of each metabolite was prepared in an appropriate solvent, in order to optimize the mass spectrometry parameters on the API 4000 Qtrap

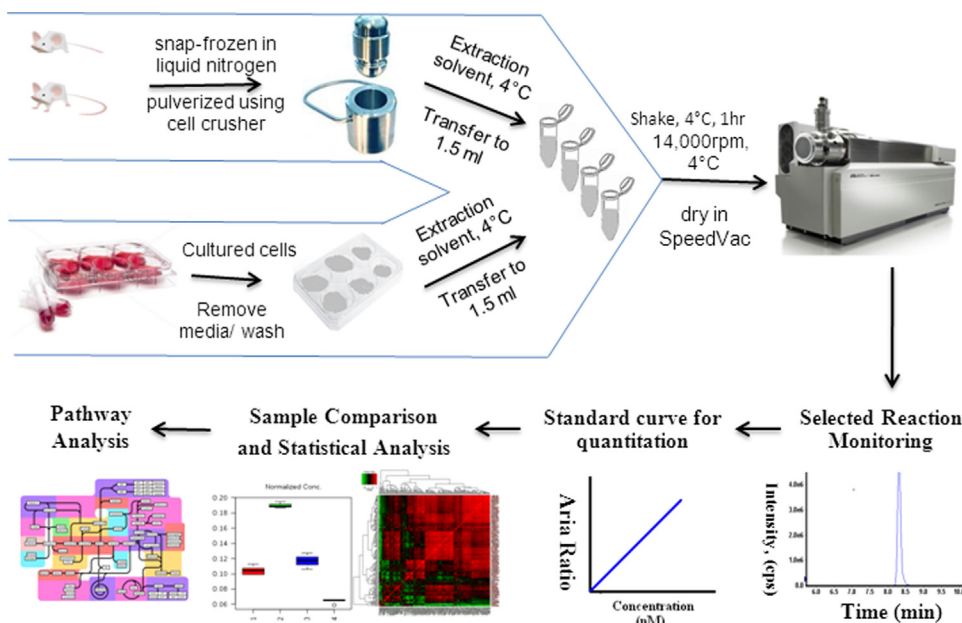


Fig. 1. Workflow for targeted LC–MS/MS analysis of hydrophilic metabolites extracted from cultured cells or tissues. Tissue samples were frozen on dry ice, stored at $-80^{\circ}C$, and crushed in a crucible on liquid nitrogen just prior to extraction. The results are normally presented as metabolite area ratios corrected by internal standard.

(AB Sciex, ON, Canada). For tuning, the infused metabolite solutions were exposed to 4500 V as ion source potential (ISP) in both positive and negative modes. The nebulizer gas (GS1) and bath gas (GS2) were 10 psi, curtain gas (CUR) was 15 psi, and collision gas (CAD) was 4 psi. Source temperature (TEM) was set to zero and the interface heater was on. The metabolite specific mass spectrometric parameters, i.e. ionization polarity, de-clustering potential (DP), precursor ion (Q1), product ion (Q3), and collision energy (CE) were obtained for each. A chromatographic method was developed to accommodate the separation of all the targeted metabolites within 20 min of run time in both polarity detection modes. A cocktail solution of these metabolites was prepared at 10 μ M each, and used to prepare a wide range calibration curve (1–1000 nM) and a set of quality control samples (30, 200, 800 nM). The mass spectrometer was maintained using a calibration kit and protocols recommended by the manufacturer (AB Sciex, ON, Canada).

2.3. Cell culture and liver tissue handling

Three cell lines were used in this method: human cervical cancer (HeLa), human embryonic kidney (Hek293), and p53 null mouse embryonic fibroblast (MEF). These cells were cultured in Dulbecco's Modified Eagle Medium (DMEM) with 4 mM L-glutamine, 25 mM D-glucose, containing 10% Fetal Bovine Serum (FBS), and were incubated in 5% CO₂ at 37 °C in 6-well cell culture non-pyrogenic polystyrene plates (6-WP). Each cell type was seeded in 6-WP and after 24 h of incubation, the media was aspirated, cells washed on the plates with warm phosphate buffered saline (PBS), and then snap-frozen in liquid nitrogen for metabolism quenching.

Liver tissue was harvested from three adult C57BL/6 male littermate mice following protocols approved by Toronto Centre for Phenogenomics. Tissues were frozen on dry ice immediately after dissection, and stored at –80 °C. All tissues were processed at the same time as follows: ~100 mg of tissue was pulverized in a cell crusher after pre-cooling in liquid nitrogen and stored at –80 °C until extraction.

2.4. Extraction of cellular and tissue metabolites

The polar cellular and liver tissue metabolites were extracted by addition of 1 mL solution of extraction solvent (40% acetonitrile, 40% methanol, and 20% water). After addition of the extraction solvent, cells were scraped and the cell/solvent mixture transferred to a 1.5 mL tube and shaken at 1000 rpm for 1 h at 4 °C in a ThermoMixer (Eppendorf, Germany). For tissue, pre-weighed liver tissue (~100 mg per sample) was pulverized in a cell crusher, which reduces most tissues to a fine, easily recoverable powder under liquid nitrogen conditions. Then the extraction solvent was added as described above for cells. Following extraction, samples were spun down at 14,000 rpm for 10 min at 4 °C, and the supernatant transferred to fresh tubes to be evaporated to dryness in a CentreVap concentrator at 40 °C (Labconco, MO). The dry extract samples were stored at –80 °C for later LC–MS/MS analysis.

2.5. LC–MS/MS analysis

The dry extracts were reconstituted in 100 μ L of water containing internal standards (500 μ g/mL and 300 μ g/mL of D₇-glucose and ¹³C₉¹⁵N-tyrosine, respectively) and then injected twice, for positive and negative MS detection modes, through HPLC (Dionex Corporation, CA) in gradient reversed phase chromatography. The metabolites were separated at room temperature through a guard column (Inertsil ODS-3, 4 mm

internal diameter \times 10 mm length, 3 μ M particle size) and analytical column (Inertsil ODS-3, 4.6 mm internal diameter, 150 mm length, and 3- μ M particle size) for both polarity modes. In positive mode analysis, the mobile phase was composed of (A) 0.1% acetic acid and (B) acetonitrile, where the acetonitrile composition was ramping from 5% to 90% in 16 min, then held for 1 min at 90%, subsequently returning within 2 min to 5% acetonitrile in mobile phase for column regeneration. In negative mode, the mobile phase was composed of (A) 0.1% tributylamine, 0.03% acetic acid, 10% methanol and (B) acetonitrile, where the acetonitrile composition was ramping from 5 to 90% in 10 min, then held for 1 min at 90%, subsequently the gradient ramped back to 5% acetonitrile in mobile phase (A), to regenerate the column for the next run. The total runtime for each sample in both modes was 20 min at flow rate 0.5 mL/min. The samples were stored at 4 °C in the auto-sampler, and the injection volume was 10 μ L. An automated washing procedure was developed before and after each sample to avoid any sample carryover.

The eluted metabolites were analyzed at the optimum mass spectrometric conditions listed in Table S1 using an electrospray ionization–triple–quadrupole mass spectrometer (AB Sciex 4000 Qtrap, Toronto, ON, Canada). The mass spectrometric data acquisition time for each run was 20 min, and the dwell time for each MRM channel was 10 ms. Common mass spectrometric parameters were the same as tuning conditions described above, except: GS1 and GS2 were 50 psi; CUR was 20 psi, and CAD was 3 and 7 for positive and negative modes, respectively, and source temperature (TEM) was 400 °C.

2.6. Assay validation

Validation of the analytical method was performed according to the American and European Food and Drug Administration (FDA) guidelines [25].

2.7. Specificity

For target metabolites and internal standards (IS), the method specificity was studied in three different batches of cell extracts. Cell extracts were spiked with stock solution of the metabolic mixture at three different concentrations, higher than the lower limit of quantification (LLOQ), and spiked with labeled IS.

2.8. Linearity and Sensitivity

For metabolites listed in Table S2, calibration curves were prepared daily in a serial dilution and spiked with IS. In each detection mode, one IS was used to correct the sample preparation and LC–MS/MS fluctuations. For linearity evaluation, three different calibration curves were prepared for each metabolite on three consecutive days. A blank, blank with IS, and 7–10 calibration curve points were analyzed using the developed method. The calibration curves were drawn by plotting the peak area ratio of analyte to IS versus the nominal concentration of each analyte. The LLOQ was defined as the lowest calibration curve point, at least ten-times greater than blank signal, and with accuracy within 80–120%, and variability less than or equal to 20% on a day-to-day basis.

2.9. Intra- and inter-day precision

The intra-day variability was evaluated by freshly preparing three independent replicates ($n=3$) of quality control (QC) samples, a mixture of standard metabolites prepared in the lab to yield concentrations of 30, 200, 800 nM. On three different

Table 1

List of targeted metabolic pathways and their experimental coverage using tandem mass spectrometry.

Metabolic pathway	Total metabolites	Measured metabolites	Coverage %
Citric acid cycle	23	18	78.3
Protein biosynthesis	19	16	84.2
Purine metabolism	45	16	35.6
Gluconeogenesis	27	15	55.6
Urea cycle	20	14	70
Ammonia recycling	18	12	66.7
Pyrimidine metabolism	36	11	30.6
Glutamate metabolism	18	10	55.6
Glycolysis	21	10	47.6
Insulin signalling	19	9	47.4
Arginine and proline metabolism	26	9	34.6
Valine, leucine and isoleucine degradation	36	8	22.2
RNA transcription	9	7	77.8
Glucose-alanine cycle	12	7	58.3
Pyruvate metabolism	20	7	35
Methionine metabolism	24	7	29.2
Alanine metabolism	6	6	100
Malate-aspartate shuttle	8	6	75
Beta-alanine metabolism	13	6	46.2
Phenylalanine and tyrosine metabolism	13	6	46.2
Amino sugar metabolism	15	6	40
Mitochondrial electron transport chain	15	6	40
Ketone body metabolism	10	5	50
Aspartate metabolism	12	5	41.7
Pentose phosphate pathway	18	5	27.8
Fructose and mannose degradation	18	5	27.8
Galactose metabolism	25	5	20
Glycine, serine and threonine metabolism	26	5	19.2
Intracellular signalling through prostacyclin receptor and prostacyclin	6	4	66.7
Intracellular signalling through adenosine receptor A2a and adenosine	7	4	57.1
Nicotinate and nicotinamide metabolism	13	4	30.8
Propanoate metabolism	18	4	22.2
Tryptophan metabolism	34	4	11.8
Tyrosine metabolism	38	4	10.5
Thiamine metabolism	4	3	75
Intracellular signalling through FSH receptor and follicle stimulating hormone	4	3	75
Excitatory neural signalling through 5-HTR 4 and serotonin	5	3	60
Corticotropin activation of cortisol production	5	3	60
Vasopressin regulation of water homeostasis	5	3	60
Intracellular signalling through histamine H2 receptor and histamine	5	3	60
Intracellular signalling through PGD2 receptor and prostaglandin D2	5	3	60
Butyrate metabolism	9	3	33.3
Glutathione metabolism	10	3	30
Histidine metabolism	11	3	27.3
Lysine degradation	13	3	23.1
Oxidation of branched chain fatty acids	14	3	21.4
Beta oxidation of very long chain fatty acids	14	3	21.4
Starch and sucrose metabolism	14	3	21.4
Inositol metabolism	19	3	15.8
Cysteine metabolism	8	2	25
Nucleotide sugars metabolism	9	2	22.2
Pantothenate and CoA biosynthesis	10	2	20
Sphingolipid metabolism	15	2	13.3
Fatty acid metabolism	29	2	6.9
Bile acid biosynthesis	49	2	4.1
Biotin metabolism	4	1	25
Phenylacetate metabolism	4	1	25
Catecholamine biosynthesis	5	1	20
Taurine and hypotaurine metabolism	7	1	14.3
Glycerol phosphate shuttle	8	1	12.5
Vitamin B6 metabolism	10	1	10
Ubiquinone biosynthesis	10	1	10
Betaine metabolism	10	1	10
Selenoamino acid metabolism	15	1	6.7
Folate and pterine biosynthesis	17	1	5.9
Phospholipid biosynthesis	19	1	5.3
Steroid biosynthesis	31	1	3.2

days, the inter-day validation was monitored using three replicates of QC samples. The accuracy was calculated as: (mean found concentration/nominal concentration) × 100%, and the variability was represented as percent relative standard deviation (%RSD).

2.10. Stability

To study metabolite and IS stability under sample preparation and analysis conditions, sets of two QC samples (200 and 800 nM) were prepared and treated under the following conditions: room

temperature (RT) for 2, 6, 24 h or 7 days, or in the auto-sampler at 4 °C for 3 days, or in an incubator at 40 °C overnight, all followed by storage at –80 °C. The molecular stability was calculated as: (area ratio of examined sample/area ratio of fresh sample) × 100%.

2.11. Data acquisition, processing, and visualization

The sample delivery to the mass spectrometer was managed through the HPLC software Chromeleon Client version 6.8 (Dionex Corporation, CA), while the MS was controlled by Analyst version 1.5.2 (AB Sciex, Toronto, ON, Canada) for sample tuning and acquisition. The peak integration and data analysis was performed using MultiQuant version 2.0.0 (AB Sciex, ON, Canada). Area under the peak was used as the quantitative measurement for assay performance in terms of linearity, sensitivity, and reproducibility.

The results table contains the samples, metabolite area ratios, and retention times. The results are normalized to cell number or protein content for cells, and tissue weight for liver samples. The actual biological sample results table was uploaded to Agilent Mass Profiler Professional software (Agilent, CA) for multivariate statistical and pathway analysis.

2.12. Application of analysis to biological samples

The validated method was applied to relatively quantify metabolic levels in three different cell lines: HeLa, Hek293, and

MEF, and liver tissues of three littermate mice. To minimize biological and procedural variability, all replicates for liver tissue and each cell line were harvested on the same day, but extracted and processed on three separate days, to test the reproducibility and reliability of the method. Subsequently, the samples were run on the same day to minimize the variability of the instrument on day-to-day runs. Thus, the day-to-day variation in extraction was studied in these biological models. The data from these samples were combined and statistically analyzed using correlation coefficient, coefficient of determination, and principle component analysis (PCA) [23].

3. Results and discussion

3.1. Method development and mass spectrometry optimization

In this study, ~150 metabolites were obtained from commercial sources and used to optimize the chromatography and mass spectrometry conditions for selective reaction monitoring, and to generate standard curves. The list of targeted pathways and the coverage of metabolites therein are summarized in Table 1. The mass spectrometer was tuned to detect specific metabolites eluted from regular reversed-phase or ion pairing reversed-phase chromatographies in positive and negative detection modes, respectively. The elution time and MS parameters, DP, Q1 (precursor ion), Q3 (product ion), CE, and CXP are summarized

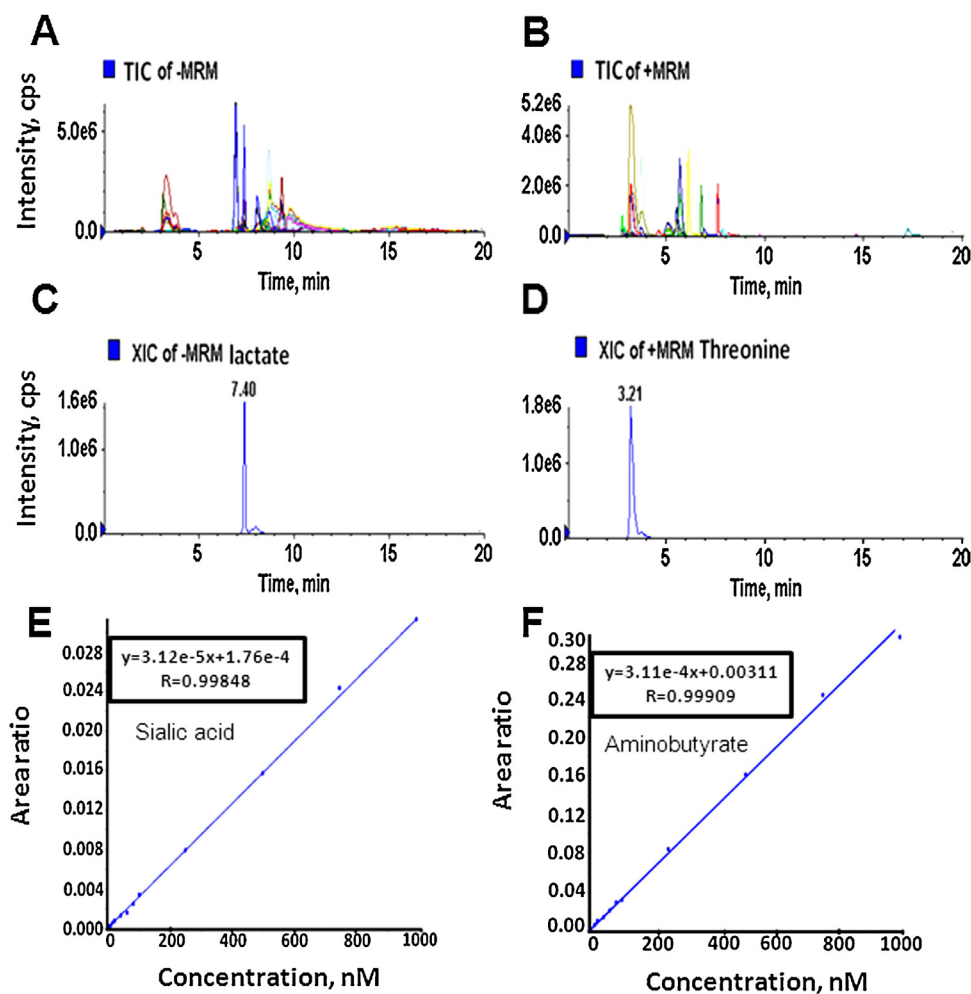


Fig. 2. Metabolite quantification. Total ion chromatograms (TIC) of metabolites extracted from HeLa cells separated by reversed phase liquid chromatography and ionized in (A), negative mode with ion-pairing reagent, and (B), positive mode. Extracted ion chromatograms (XIC) from (C), negative mode (lactate) and (D), positive mode (threonine). Linear calibration curves for (E), sialic acid (negative mode), and (F), aminobutyrate (positive mode).

in supplementary Table S1. The glycolysis, citric acid cycle, pentose phosphate pathway, hexosamine biosynthetic pathway, and other sugar-based metabolites were separated by ion-pairing reversed phase chromatography to obtain a sharp peak that gave resolution between adjacent peaks for some isobaric molecules. The chromatographic parameters were developed after mobile phase optimization in terms of composition (gradient regime), pH for the ion pairing part, and flow rate. The sharpness and resolution of the analytical peak is the guidance for optimizing the chromatographic conditions. The reproducibility of liquid chromatography is very important to distinguish between endogenous molecules and artifacts produced inside the ion source such as ATP dissociation to ADP and/or AMP. Representative total ion chromatograms (TIC) in both positive and negative detection modes are shown in Fig. 2A and B, and examples of extracted ion chromatograms (XIC) for lactate and threonine are displayed in Fig. 2C and D. A dilution series for each metabolite was run, and the analyte area/internal standard ratio versus its nominal concentration was analyzed for linearity by least-squares regression with weighting $1/x$ (Fig. 2E and F). The mean Pearson correlation coefficient of determination

(R^2), determined over the course of several days was greater than 0.99 for all the metabolites tested (Table S2).

3.2. Sensitivity and specificity

Under optimized LC–MS/MS conditions, samples extracted from cells and tissues showed no significant interfering peaks at the retention times of each metabolite. The sensitivity of the method was evaluated as described in the methodology section, at a concentration three times above the lower limit of quantification (LLOQ), which are reported in Table S2. The LLOQ values are the average of the lowest point in each valid calibration curve with relative standard deviation (RSD) ranging between 80 and 120%. Sensitivities for each metabolite varied over a wide range, as it depends on the molecular proton affinity under the common mass spectrometric parameters such as ion source gas pressure and temperature, collision energy, and the post-source chemical stability. Under the optimum chromatographic conditions, peaks of the targeted metabolites were adequately separated at retention time ranges from 1.5 to 14.0 min.

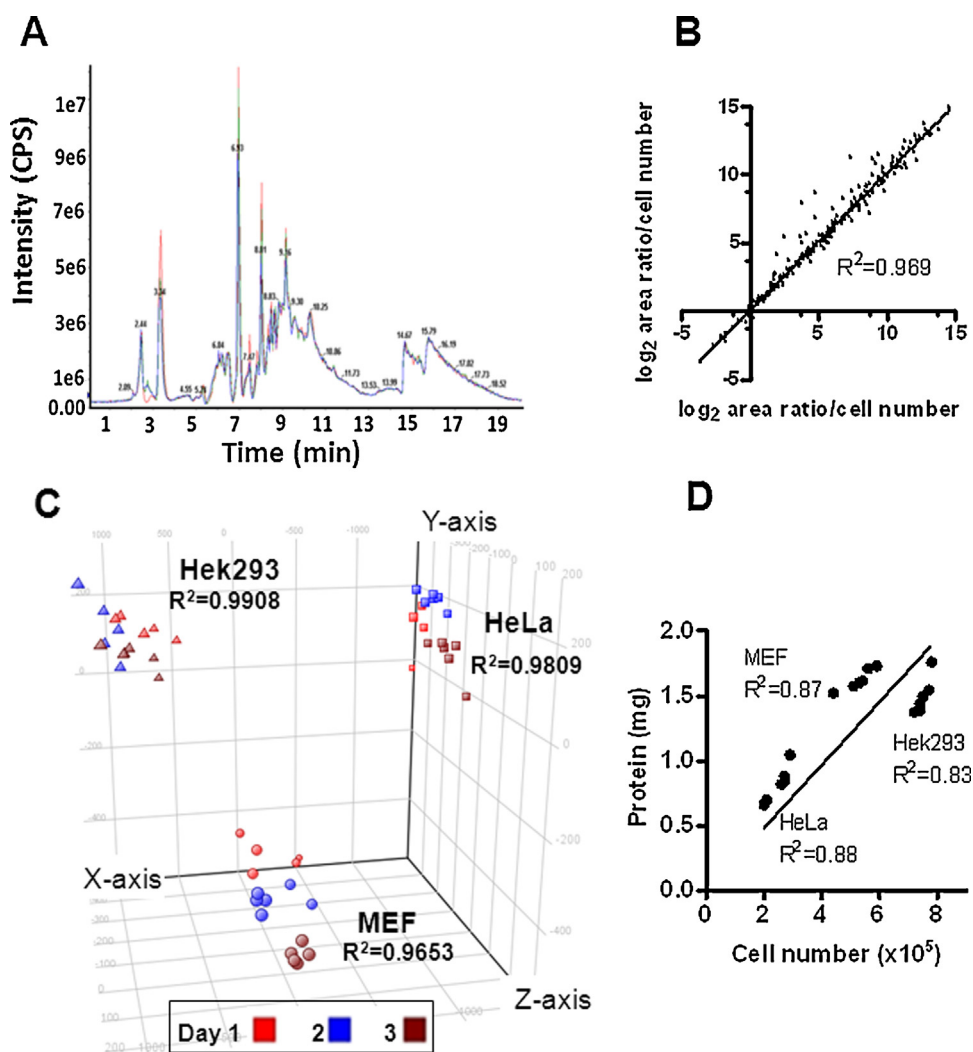


Fig. 3. Reproducibility of metabolic profiles from three cell lines. (A) An overlaid TIC chromatogram of three identical HeLa cell extracts prepared on three consecutive days, labeled blue, red and green; intensity in counts per second. (B) Example of concordance of metabolite data from HeLa cell extracts prepared on 2 separate days. (C) Principal component analysis of data for three cell lines (HeLa, Hek293, and MEF) analyzed on three consecutive days, with plots of five technical replicates on each day. The coefficient of determination (R^2) between separate days for each cell line was >0.96 . The metabolite peak area ratios were normalized to cell number. (D) Cell number at harvest and protein content in lysates of five replicate samples, with R^2 displayed for each cell line, and for combined (line) being 0.66, reflecting greater variation between the cell lines than within each one. (For interpretation of the references to colour in this figure legend, the reader is referred to the web version of this article.)

3.3. Intra- and inter-day accuracy and precision

The (inter- and intra-day) precision and accuracy were evaluated for the listed metabolites at three concentrations of quality control (QC) samples (low QC, medium QC, and high QC). The inter-day variability for all compounds was less than 15%, and inter-day accuracy ranged from 85 to 115% (Table S3) for the QCs, which meets the criteria of a validated bioanalytical method to be utilized routinely for metabolomic quantitative profiling. The reproducibility of data acquired from biological samples was demonstrated by overlapped TIC chromatograms of HeLa cell extracts obtained from three separate extractions, as shown in Fig. 3. The day-to-day coefficient of determination (R^2) was 0.9809.

3.4. Stability

The samples were stored at -80°C for LC-MS/MS analysis. The stability of targeted metabolites was studied under different preparation and acquisition conditions using the medium and high levels of QC samples. Equivalent samples of the standards were removed from -80°C and left at RT for 2, 6, 24 h or 7 days, in the auto-sampler at 4°C for 3 days, or in an incubator at 40°C overnight to simulate the SpeedVac conditions where the extraction solvents were evaporated. The stability of each metabolite was evaluated relative to freshly prepared samples stored at -80°C , and are summarized in Table S4. The bench-top stability of compounds showed only a slight reduction between 2 h and 6 h, but was very poor after 24 h (data not shown). Some compounds were fairly

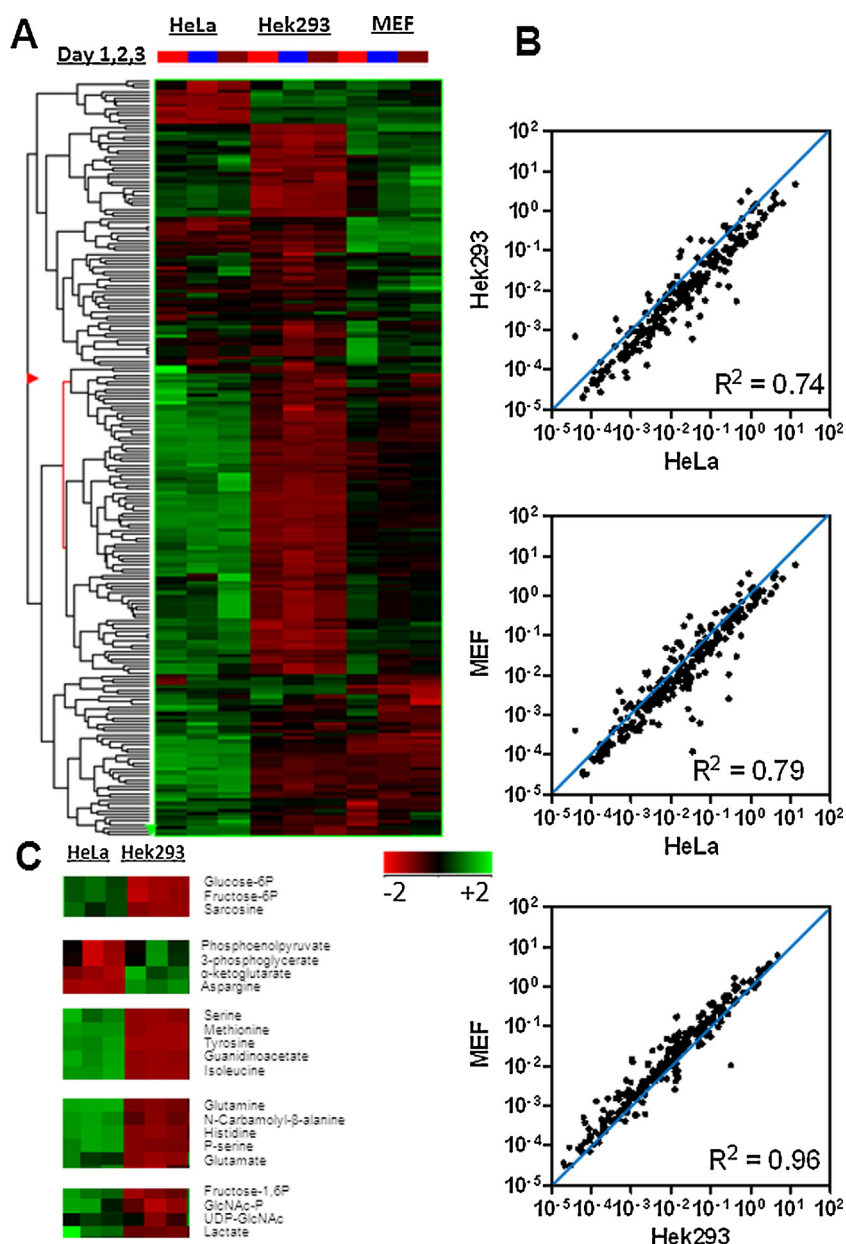


Fig. 4. Metabolic profiles reveal sensitivity and cell-type specific features. (A) Heat maps comparing HeLa, Hek293 and MEFs ($n = \text{mean of 5 replicates/day, over 3 days}$). (B) Two-way comparison of area ratios/cell number for HeLa, Hek293 and MEFs. (C) Selected portions of the HeLa and Hek293 heat map that exhibit some of the known cancer-associated metabolic alterations, as described in the text.

unstable compared to the internal standard, which supports the idea of having more IS compounds that have closer structural features to the target metabolites. In general, most metabolite stability under these conditions ranged between 70 and 130%, except overnight at room temperature (24 h), where the stability for some metabolites dropped below 60%. The results for the molecules within these ranges of stability are considered valid to be reported because the area of the LLOQ is still 10 fold above the noise and the RSD ranges between 80 and 120%.

Biological samples are a complex matrix from which metabolites must be extracted. The efficiency of extraction can vary between metabolites and various biological matrixes. We optimized the extraction solvent used on cells and tissues in terms of organic-to-aqueous ratio, solvent pH, and polarity to minimize extraction loss and maximize LLOQ signal for most metabolites investigated. Profiling of biological samples are often comparative studies, but when concentrations are required, a heavy-labeled version of the metabolite should be added before extraction as a control.

3.5. Sensitivity and precision with biological samples

Human cervical cancer (HeLa), human embryonic kidney (Hek293), and p53-deficient mouse embryonic fibroblast (MEF) cells were cultured under the same conditions for 24 h followed by quenching and extraction of metabolites, which were subsequently dried and stored at -80°C prior to LC–MS/MS analysis. The extraction procedure was performed on replicate samples on three consecutive days to address the non-biological variation, and to validate the method's reproducibility. The metabolite peak areas per 10^6 cells were used to generate a principle component analysis (PCA) plot, which revealed clustering by cell type, indicating that variation between cell lines can be readily detected (Fig. 3C). Moreover, non-biological variation was low, as indicated by clustering on a much smaller scale based on the day of extraction. Cell number and protein content correlated well, indicating that normalization will generally be similar by either measure (Fig. 3D).

The reproducibility of replicates and difference between the three cell lines is observed in an unsupervised hierarchical clustering represented as a heat map (Fig. 4A). Pair-wise comparison of the three cell lines, revealed the best multiple correlation coefficient ($R^2 = 0.96$) for the non-transformed mouse MEF and Hek293 cell lines, while comparison of these cell lines with HeLa cells showed weaker correlation (Fig. 4B), as also reflected visually in the accompanying heat maps. This suggests

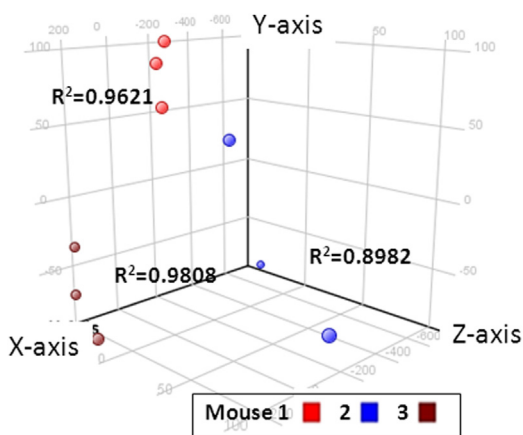


Fig. 5. Reproducibility of metabolic profiles from liver extracts. Metabolic data was collected from three aliquots of liver tissues from three different mice, stored at -80°C and extracted on three consecutive days. Principal component analysis reveals mouse-dependent clustering, thus illustrating reproducibility that can distinguish the three cage littermates.

that cancer-associated changes in metabolism should be present in the comparisons between human HeLa and Hek293 cells. Metabolic reprogramming in cancer cells results in increased uptake of glucose, glutamine and essential amino acids, which support anabolic pathways [6]. Indeed, comparing the human cell lines, malignant HeLa and immortalized Hek293, we observed expected features of metabolic reprogramming in HeLa cells [26] (Fig. 4C). This includes increased glucose-6P, fructose-6P and lactate, but lowered phosphoenolpyruvate and 3-phosphoglycerate, downstream intermediates that are precursors to phosphoserine in serine–glycine pathway [10,12], as well as sarcosine [17]. Glutamine and glutamate were also increased, while α -ketoglutarate was lower, reflecting the need for anaplerosis in the citric acid cycle [27,28]. The branched-chain essential amino acids isoleucine and leucine activate mTor and promote cell growth [29]. The levels of GlcNAc-P and UDP-GlcNAc were also increased in HeLa cells, consistent with increased activity of the hexosamine biosynthesis pathway [3,30] supplying UDP-GlcNAc to protein glycosylation required for cancer progression [31].

3.6. Reproducibility in metabolite profiles can distinguish individual animals

Livers were collected from three wild-type male littermate mice, and three pieces from each liver were snap frozen and stored at -80°C . Metabolites were extracted from the liver of each mouse on three consecutive days, and all were analyzed by LC–MS/MS on the same day (Fig. 5). Since mice were fed *ad libitum*, the profile of liver metabolites may reflect the differences in how much and when each mouse last consumed food. Indeed, the triplicate samples clustered in PCA primarily by the mouse from which the metabolites came, confirming the sensitivity and reproducibility of our method.

4. Conclusion

We anticipate that this method will be widely applicable to groups wishing to undertake metabolic profiling of cells or tissues. We note that ion-pairing agents such as tributylamine are often avoided for use in positive mode LC–MS due to their potential for ion suppression. In this application on a triple quadrupole instrument, we observe excellent sensitivity, and designed our transitions to avoid the detection of the tributylamine ion. The great retention of polar compounds in this ion paired method provides excellent selectivity for mass spectrometry.

Acknowledgments

Research described in this manuscript was supported by grants from Canadian Cancer Society (2010-7000444), MRI-ORF GL2, CIHR (MOP-62975), and The Sydney C. Cooper Program for the Prevention of Cancer Progression to J.W.D. A.A.R was supported by MITACS-Accelerate, and M.R. was supported by the Frank Fletcher Memorial Fund, Mary Gertrude l'Anson Scholarship, and Paul Starita Graduate Student Fellowship. AAC is the Canada Research Chair in Metabolomics for Enzyme Discovery and is supported by the Ontario Early Researcher Award, by the Canadian Institutes for Health Research, and by the Natural Sciences and Engineering Research Council of Canada, and by the Canadian Foundation for Innovation and the Ontario Leader's Opportunity Fund.

Appendix A. Supplementary data

Supplementary data associated with this article can be found in the online version at <http://dx.doi.org/10.1016/j.aca.2014.06.012>.

References

- [1] R. Madsen, T. Lundstedt, J. Trygg, Chemometrics in metabolomics – a review in human disease diagnosis, *Anal. Chim. Acta* 659 (2010) 23–33.
- [2] J. Fan, J.J. Kamphorst, R. Mathew, M.K. Chung, E. White, T. Shlomi, J.D. Rabinowitz, Glutamine-driven oxidative phosphorylation is a major ATP source in transformed mammalian cells in both normoxia and hypoxia, *Mol. Syst. Biol.* 9 (2013) 712.
- [3] H. Ying, A.C. Kimmelman, C.A. Lyssiotis, S. Hua, G.C. Chu, E. Fletcher-Sananikone, J.W. Locasale, J. Son, H. Zhang, J.L. Coloff, H. Yan, W. Wang, S. Chen, A. Viale, H. Zheng, J.H. Paik, C. Lim, A.R. Guimaraes, E.S. Martin, J. Chang, A.F. Hezel, S.R. Perry, J. Hu, B. Gan, Y. Xiao, J.M. Asara, R. Weissleder, Y.A. Wang, L. Chin, L.C. Cantley, R.A. DePinho, Oncogenic Kras maintains pancreatic tumors through regulation of anabolic glucose metabolism, *Cell* 149 (2012) 656–670.
- [4] M.F. Clasquin, E. Melamud, A. Singer, J.R. Gooding, X. Xu, A. Dong, H. Cui, S.R. Campagna, A. Savchenko, A.F. Yakunin, J.D. Rabinowitz, A.A. Caudy, Riboneogenesis in yeast, *Cell* 145 (2011) 969–980.
- [5] O. Warburg, On the origin of cancer cells, *Science* 123 (1956) 309–314.
- [6] A.J. Levine, A.M. Puzio-Kuter, The control of the metabolic switch in cancers by oncogenes and tumor suppressor genes, *Science* 330 (2010) 1340–1344.
- [7] R.J. DeBerardinis, J.J. Lum, G. Hatzivassiliou, C.B. Thompson, The biology of cancer: metabolic reprogramming fuels cell growth and proliferation, *Cell Metab.* 7 (2008) 11–20.
- [8] A. Schulze, A.L. Harris, How cancer metabolism is tuned for proliferation and vulnerable to disruption, *Nature* 491 (2012) 364–373.
- [9] J. Kaplon, L. Zheng, K. Meissl, B. Chaneton, V.A. Selivanov, G. Mackay, S.H. van der Burg, E.M. Verdegaaal, M. Cascante, T. Shlomi, E. Gottlieb, D.S. Peeper, A key role for mitochondrial gatekeeper pyruvate dehydrogenase in oncogene-induced senescence, *Nature* 498 (2013) 109–112.
- [10] W.C. Zhang, N. Shyh-Chang, H. Yang, A. Rai, S. Umashankar, S. Ma, B.S. Soh, L.L. Sun, B.C. Tai, M.E. Nga, K.K. Bhakoo, S.R. Jayapal, M. Nichane, Q. Yu, D.A. Ahmed, C. Tan, W.P. Sing, J. Tam, A. Thirugananam, M.S. Noghabi, Y.H. Pang, H.S. Ang, W. Mitchell, P. Robson, P. Kaldis, R.A. Soo, S. Swarup, E.H. Lim, B. Lim, Glycine decarboxylase activity drives non-small cell lung cancer tumor-initiating cells and tumorigenesis, *Cell* 148 (2012) 259–272.
- [11] M. Jain, R. Nilsson, S. Sharma, N. Madhusudhan, T. Kitami, A.L. Souza, R. Kafri, M.W. Kirschner, C.B. Clish, V.K. Mootha, Metabolite profiling identifies a key role for glycine in rapid cancer cell proliferation, *Science* 336 (2012) 1040–1044.
- [12] R. Possemato, K.M. Marks, Y.D. Shaul, M.E. Pacold, D. Kim, K. Birsoy, S. Sethumadhavan, H.K. Woo, H.G. Jang, A.K. Jha, W.W. Chen, F.G. Barrett, N. Stransky, Z.Y. Tsun, G.S. Cowley, J. Barretina, N.Y. Kalaany, P.P. Hsu, K. Ottina, A. M. Chan, B. Yuan, L.A. Garraway, D.E. Root, M. Mino-Kenudson, E.F. Brachtel, E. M. Driggers, D.M. Sabatini, Functional genomics reveal that the serine synthesis pathway is essential in breast cancer, *Nature* 476 (2011) 346–350.
- [13] K. Dettmer, P.A. Aronov, B.D. Hammock, Mass spectrometry-based metabolomics, *Mass Spectrom. Rev.* 26 (2007) 51–78.
- [14] W. Weckwerth, Metabolomics in systems biology, *Ann. Rev. Plant Biol.* 54 (2003) 669–689.
- [15] S. Vo Duy, S. Besteiro, L. Berry, C. Perigaud, F. Bressolle, H.J. Vial, I. Lefebvre-Tournier, A quantitative liquid chromatography–tandem mass spectrometry method for metabolomic analysis of *Plasmodium falciparum* lipid related metabolites, *Anal. Chim. Acta* 739 (2012) 47–55.
- [16] M. Yuan, S.B. Breitkopf, X. Yang, J.M. Asara, A positive/negative ion-switching, targeted mass spectrometry-based metabolomics platform for bodily fluids, cells, and fresh and fixed tissue, *Nat. Protoc.* 7 (2012) 872–881.
- [17] A. Sreekumar, M. Poisson, M. Rajendiran, P. Khan, Q. Cao, J. Yu, B. Laxman, R. Mehra, J. Lonigro, Y. Li, K. Nyati, A. Ahsan, S. Kalyana-Sundaram, B. Han, X. Cao, J. Byun, S. Omenn, D. Ghosh, S. Pennathur, C. Alexander, A. Berger, R. Shuster, T. Wei, S. Varambally, C. Beecher, M. Chinnaiyan, Metabolomic profiles delineate potential role for sarcosine in prostate cancer progression, *Nature* (2009) 910–914.
- [18] K. Smolkova, P. Jezek, The role of mitochondrial NADPH-dependent isocitrate dehydrogenase in cancer cells, *Int. J. Cell Biol.* 2012 (2012) 273947.
- [19] R. Steuer, J. Kurths, O. Fiehn, W. Weckwerth, Interpreting correlations in metabolomic networks, *Biochem. Soc. Trans.* 31 (2003) 1476–1478.
- [20] X. Cai, L. Zou, J. Dong, L. Zhao, Y. Wang, Q. Xu, X. Xue, X. Zhang, X. Liang, Analysis of highly polar metabolites in human plasma by ultra-performance hydrophilic interaction liquid chromatography coupled with quadrupole-time of flight mass spectrometry, *Anal. Chim. Acta* 650 (2009) 10–15.
- [21] A.M. Abdel Rahman, M. Ryczko, J. Pawling, J.W. Dennis, Probing the hexosamine biosynthetic pathway in human tumor cells by multitargeted tandem mass spectrometry, *ACS Chem. Biol.* 8 (2013) 2053–2062.
- [22] A.M. Abdel Rahman, S. Gagne, R.J. Helleur, Simultaneous determination of two major snow crab aeroallergens in processing plants by use of isotopic dilution tandem mass spectrometry, *Anal. Bioanal. Chem.* 403 (2012) 821–831.
- [23] S. Dietmair, N.E. Timmins, P.P. Gray, L.K. Nielsen, J.O. Kromer, Towards quantitative metabolomics of mammalian cells: development of a metabolite extraction protocol, *Anal. Biochem.* 404 (2010) 155–164.
- [24] A.M. Abdel Rahman, A.L. Lopata, E.W. Randell, R.J. Helleur, Absolute quantification method and validation of airborne snow crab allergen tropomyosin using tandem mass spectrometry, *Anal. Chim. Acta* 681 (2010) 49–55.
- [25] F. Garofolo, J. Michon, V. Leclaire, B. Booth, S. Lowes, C.T. Viswanathan, J. Welink, S. Haidar, S. Teixeira Lde, D. Tang, B. Desilva, US FDA/EMA harmonization of their bioanalytical guidance/guideline and activities of the Global Bioanalytical Consortium, *Bioanalysis* 4 (2012) 231–236.
- [26] M.G. Vander Heiden, J.W. Locasale, K.D. Swanson, H. Sharfi, G.J. Heffron, D. Amador-Noguez, H.R. Christofk, G. Wagner, J.D. Rabinowitz, J.M. Asara, L.C. Cantley, Evidence for an alternative glycolytic pathway in rapidly proliferating cells, *Science* 329 (2010) 1492–1499.
- [27] W. Hu, C. Zhang, R. Wu, Y. Sun, A. Levine, Z. Feng, Glutaminase 2, a novel p53 target gene regulating energy metabolism and antioxidant function, *Proc. Natl. Acad. Sci. U. S. A.* 107 (2010) 7455–7460.
- [28] S. Suzuki, T. Tanaka, M.V. Poyurovsky, H. Nagano, T. Mayama, S. Ohkubo, M. Lokshin, H. Hosokawa, T. Nakayama, Y. Suzuki, S. Sugano, E. Sato, T. Nagao, K. Yokote, I. Tatsuno, C. Prives, Phosphate-activated glutaminase (GLS2), a p53-inducible regulator of glutamine metabolism and reactive oxygen species, *Proc. Natl. Acad. Sci. U. S. A.* 107 (2010) 7461–7466.
- [29] P. Nicklin, P. Bergman, B. Zhang, E. Triantafellow, H. Wang, B. Nyfeler, H. Yang, M. Hild, C. Kung, C. Wilson, V.E. Myer, J.P. Mackeigan, J.A. Porter, Y.K. Wang, L.C. Cantley, P.M. Finan, L.O. Murphy, Bidirectional transport of amino acids regulates mTOR and autophagy, *Cell* 136 (2009) 521–534.
- [30] K.S. Lau, E.A. Partridge, A. Grigorian, C.I. Silvescu, V.N. Reinhold, M. Demetriou, J.W. Dennis, Complex N-glycan number and degree of branching cooperate to regulate cell proliferation and differentiation, *Cell* 129 (2007) 123–134.
- [31] E.A. Partridge, C. Le Roy, G.M. Di Guglielmo, J. Pawling, P. Cheung, M. Granovsky, I.R. Nabi, J.L. Wrana, J.W. Dennis, Regulation of cytokine receptors by Golgi N-glycan processing and endocytosis, *Science* (2004) 120–124.

Table S1: List of targeted metabolites with their optimum LC-MS/MS conditions and corresponding databases accession numbers.

Name	RT (min)	Ionization mode	Precursor ion (m/z)	Product ion (m/z)	DP (V)	CE (eV)	HMDB	PubChem	KEGG
1,4-diaminobutane	2.4	+	87	45	41	21	HMDB01414	1045	C00134
2'-Deoxycytidine	2.8	+	228	112	111	53	HMDB00014	13711	C00881
2'-Deoxy-D-ribose	3.9	-	134	117	31	15	HMDB03224	10786	C01801
2-Ketobutyrate	1.9	+	102	94	21	11	HMDB00005	3593277	NA
4-guanidinobutyrate	2.5	+	146	87	76	25	HMDB03464	500	C01035
Acetoacetate	1.9	+	85	70	40	20	HMDB00060	96	C00164
Acetylcholine	2.5	+	147	87	25	21	HMDB00895	187	C01996
Adenosine	6.1	+	268	136	40	30	HMDB00050	60961	C00212
Aminoisobutyrate	2.4	+	104	86	40	16	HMDB01906	6119	C03665
Anthranilate	9.4	+	138	120	25	18	HMDB01123	227	C00108
Carnitine	2.5	+	163	85	25	29	METPA0048	NA	C00487
Carnosine	2.1	+	227	110	40	33	HMDB00033	439224	C00386
Creatine	3.2	+	132	90	50	17	HMDB00064	586	C00300
Creatinine	2.3	+	114	44	25	28	HMDB00562	588	C00791
Cysteine	3.2	+	122	76	25	20	METPA0075	NA	C00736
Cytidine	2.8	+	244	112	25	17	HMDB00089	6175	C00475
Cytosine	2.3	+	112	95	40	26	HMDB00630	597	C00380
U ¹³ N ¹⁵ -Tyrosine *	5.7	+	192.2	145.1	115	45	NA	NA	NA
2-Aminoadipate	3.8	+	162	98	46	25	HMDB00510	92136	C00956
Xylitol	3.4	+	153	95	41	19	HMDB02917	6912	C00379
γ-Amino(iso)butyrate	2.4	+	104	87	41	15	HMDB00112	119	C00334
Glucosamine	2.2	+	180	162	50	10	HMDB01514	439213	C00329
Gluconolactone	5.8	+	179	133	46	15	HMDB00150	7027	C00198
Guanine	4.5	+	152	135	40	30	HMDB00132	764	C00242
Guanosine	6.2	+	284	152	40	25	HMDB00133	6802	C00387
Inosine	6	+	269	137	1	15	HMDB00195	6021	C00294
Alanine	3.2	+	90	44	25	17	HMDB00161	5950	C00041
Aminoadipate	3.9	+	163	73	41	37	HMDB00510	92136	C00956
Aminobutyrate	3.3	+	104	58	30	17	HMDB00452	80283	C02356
Arginine	2.8	+	175	70	25	32	HMDB00517	6322	C00062
Asparagine	3.2	+	133	74	30	23	HMDB00168	6267	C00152
Aspartate	6.3	+	134	74	25	21	HMDB00191	5960	C00049
Canavanine	2.1	+	177	76	56	35	HMDB02706	NA	C00308
Carnitine	2.5	+	162	103	86	25	HMDB00062	2724480	C00318
Citrulline	3.2	+	176	70	41	27	HMDB00904	9750	C00327
Cystine	2.1	+	241	109	46	37	HMDB00192	67678	C00491

Name	RT (min)	Ionization mode	Precursor ion (m/z)	Product ion (m/z)	DP (V)	CE (eV)	HMDB	PubChem	KEGG
Glutamate	3.8	+	148	84	25	23	HMDB00148	33032	C00025
Glutamine	3.2	+	147	84	25	25	HMDB00641	5961	C00064
Histidine	2.1	+	156	110	25	21	HMDB00177	6274	C00135
Homoserine	3.2	+	120	74	50	40	HMDB00719	12647	C00263
Lipoamide	7.5	-	206	189	41	15	HMDB00962	863	C00248
Isoleucine	4.8	+	132	86	50	18	HMDB00172	791	C00407
Leucine	5.6	+	132	86	50	18	HMDB00687	6106	C00123
Lysine	2.1	+	147	84	25	25	HMDB00182	5962	C00047
Methionine	4.6	+	150	61	40	31	HMDB00696	6137	C00073
Phenylalanine	6.7	+	166	120	50	19	HMDB00159	6140	C00079
Proline	3.5	+	116	70	50	20	HMDB00162	145742	C00148
Serine	3.2	+	106	60	25	18	HMDB00187	5951	C00065
Threonine	3.2	+	120	74	50	20	HMDB00167	6288	C00188
Tyrosine	5.6	+	182	136	25	19	HMDB00158	6057	C00082
Valine	3.7	+	118	72	25	18	HMDB00883	1182	C00183
Mevalonolactone	6.9	+	131	69	41	19	HMDB06024	10428	NA
Niacinamide	6	+	123	80	30	30	HMDB01406	936	C00153
Hydroxyproline	3.3	+	132	86	50	18	HMDB00725	5810	C01157
Ornithine	2	+	133	70	16	31	HMDB00214	6262	C00077
phosphoethanolamine	3.2	+	142	44	50	20	HMDB00224	1015	C00346
Pyridoxal	3	+	168	150	51	79	HMDB01545	1050	C00250
S-(2-Aminoethyl)-L-cysteine	2	+	165	120	46	19	HMDB33518	16218879	NA
Spermidine	1.9	+	146	72	46	18	HMDB01257	1102	C00315
Spermine	1.9	+	203	129	40	25	HMDB01256	1103	C00750
Taurine	3.3	+	126	108	50	20	HMDB00251	1123	C00245
Thiamine	2.8	+	265	122	46	18	HMDB00235	1130	C00378
Thiamine monophosphate	2.3	+	345	122	66	29	HMDB02666	1131	C01081
Thymidine	6.8	+	243	127	30	35	HMDB00273	5789	C00214
Thymine	6.5	+	127	110	40	16	HMDB00262	1135	C00178
Trans-4-hydroxy-L-Proline	3.3	+	132	68	66	23	HMDB00725	5810	C01157
Uracil	5.3	+	113	70	71	29	HMDB00300	1174	C00106
Uridine	5.9	+	245	113	96	25	HMDB00296	6029	C00299
Xanthine	5.9	+	153	110	40	21	HMDB00292	1188	C00385
2,3-Dihydroxybenzoate	8.8	-	153	109	-45	-30	HMDB00397	19	C00196
2,3-Pyridinedicarboxylate	5	-	166	122	-110	-54	HMDB00232	1066	C03722
2-Oxobutyrate	8.1	-	101	57	-30	-10	HMDB00005	58	C00109
3-Indoleacetate	8.1	-	174	130	-25	-14	HMDB00197	802	C00954
4-Aminobenzoate	7.8	-	136	92	-40	-14	HMDB01392	978	C00568
4-Hydroxybenzoate	7.9	-	137	93	-20	-20	HMDB00500	135	C00156

Name	RT (min)	Ionization mode	Precursor ion (m/z)	Product ion (m/z)	DP (V)	CE (eV)	HMDB	PubChem	KEGG
4-Hydroxyphenylpyruvate	3.3	-	179	107	-110	-54	HMDB00707	979	C01179
5-hydroxyindole-3-acetate	7.2	-	190	146	-50	-16	HMDB00763	1826	C05635
Acetyl Co-enzyme A	8.7	-	808	159	-150	-88	HMDB01206	6302	C00024
Adenine	5.5	-	134	107	-65	-24	HMDB00034	190	C00147
Adenosine 5'-monophosphate	3.3	-	346	79	-30	-66	HMDB00045	6083	C00020
Adenosine diphosphate	8.6	-	426	159	-75	-36	HMDB01341	6022	C00008
Adenosine triphosphate	8.6	-	506	159	-100	-44	HMDB00538	5957	C00002
α -ketoglutarate	8.2	-	145	101	-20	-12	HMDB00208	51	C00026
β -hydroxypyruvate	7.3	-	103	59	-20	-14	HMDB01352	135653531	NA
Aconitate	8.3	-	173	85	-25	-16	HMDB00072	309	C00417
Citrate	8.7	-	191	111	-25	-18	HMDB00094	311	C00158
Co-enzyme A	8.7	-	766	159	-135	-86	HMDB01423	6816	C00010
Creatine phosphate	8	-	210	79	-35	-24	HMDB01511	5359254	C02305
Cytidine monophosphate	7.5	-	322	139	-70	-32	HMDB00095	6131	C00055
D7-Glucose*	3.4	-	186	124	-55	-12	NA	NA	NA
Arabino-1,4-lactone	7.7	-	147	59	-55	-18	METPA0132	NA	C01114
Isocitrate	8.7	-	191	111	-35	-20	HMDB00193	1198	C00311
Maltose	3.2	-	341	161	-40	-12	HMDB00163	439186	C00208
Rib(ul)ose-5-Phosphate	7.5	-	229	79	-15	-58	HMDB01548	77982	C00117
Xylose	3.4	-	149	89	-50	-8	HMDB00098	135191	C00181
Fructose 1,6-bisphosphate	8.3	-	339	241	-30	-22	HMDB01058	718	C00354
Fructose 6-phosphate	6.9	-	259	169	-50	-18	HMDB00124	69507	C00085
Fumarate	8.1	-	115	71	-30	-10	HMDB00134	723	C00122
Glucosamine	3.5	+	178	145	-30	-12	HMDB01514	439213	C00329
Glucosamine 6-Phosphate	4.1	-	258	97	-75	-18	HMDB01254	439217	C00352
Glucose	3.3	-	179	119	-60	-12	HMDB00122	5793	C00031
Glucose 6-Phosphate	6.9	-	259	199	-55	-16	HMDB01401	208	C00668
Glyoxylate	7.4	-	73	45	-45	-10	HMDB00119	760	C00048
Guanosinediphosphate	8.7	-	442	159	-75	-38	HMDB01201	8977	C00035
Guanosinediphosphate- Fucose	8	-	588	159	-100	-60	HMDB01095	27505	C00325
Guanosinediphosphate-Mannose	8.7	-	604	159	-120	-70	HMDB01163	732	C00096
Guanosine monophosphate	7.5	-	362	79	-70	-60	HMDB01397	6804	C00144
Guanosinetriphosphate	8.8	-	522	159	-95	-48	HMDB01273	6830	C00044
Hypoxanthine	4.8	-	135	92	-30	-22	HMDB00157	790	C00262
Inosine 5'-monophosphate	7.7	-	347	79	-65	-100	HMDB00175	8582	C00130
Itaconate	8.2	-	129	85	-40	-12	HMDB02092	811	C00490
Sorbose	3.3	-	179	89	-40	-12	HMDB01266	439192	C00247
Fucose	3.7	-	163	103	-55	-10	HMDB00174	17106	C01019
Lactate	3.4	-	89	71	-55	-16	HMDB00190	107689	C00186

Name	RT (min)	Ionization mode	Precursor ion (m/z)	Product ion (m/z)	DP (V)	CE (eV)	HMDB	PubChem	KEGG
Malate	9	-	133	115	-40	-14	HMDB00156	222656	C00149
Malonyl Co-enzyme A	8.7	-	852	159	-130	-96	HMDB01175	10663	C00083
Melibiose	3.2	-	341	89	-50	-28	HMDB00048	440658	C05402
myo-inositol	3.2	-	179	87	-65	-26	HMDB00211	892	C00137
N-acetylglucosamine	3.5	-	220	119	-60	-10	HMDB00215	439174	C00140
N-acetylglucosamine phosphate	7	-	300	199	-75	-20	HMDB02817	150941	NA
N-Acetylglutamate	8.1	-	188	143	-35	-18	HMDB01138	185	C00624
NADH	8.1	-	664	408	-130	-46	HMDB01487	928	C00004
Nicotinamide adenine dinucleotide	6.9	-	662	540	-90	-28	HMDB00902	5892	C00003
Nicotinate	7.8	-	122	78	-35	-18	HMDB01488	938	C00253
hydroxyphenylpyruvate	3.3	-	179	107	-40	-12	HMDB00205	997	C00166
o-Phosphoryl-ethanol-amine	4.7	-	140	79	-110	-54	HMDB00224	1015	C00346
Oxaloacetate	8.7	-	133	87	-30	-12	HMDB00223	970	C00036
Oxidized glutathione	7.8	-	611	306	-60	-60	HMDB03337	975	C00127
Pantothenate	7.5	-	218	88	-55	-22	HMDB00210	6613	C00864
Phenylpyruvate	9.5	-	163	91	-25	-14	HMDB00205	997	C00166
Phosphoenolpyruvate	8.5	-	167	79	-40	-31	HMDB00263	1005	C00074
Phosphotyrosine	11.1	-	260	79	-50	-30	HMDB06049	30819	C06501
Phytate	11.6	-	329	79	-40	-98	HMDB03502	890	C01204
Pyruvate	7.7	-	87	43	-35	-10	HMDB00243	1060	C00022
Quinolate	9.1	-	166	122	-30	-13	HMDB00232	1066	C03722
Reduced glutathione	7	-	306	143	-40	-32	HMDB00125	124886	C00051
Shikimate	8.9	-	173	93	-25	-20	HMDB03070	8742	C00493
Sialate	7	-	308	170	-50	-22	HMDB00230	439197	C00270
Succinate	8	-	117	73	-30	-16	HMDB00254	1110	C00042
Succinyl Co-enzyme A	8.8	-	866	159	-135	-90	HMDB01022	439161	C00091
Thiamine pyrophosphate	3.6	-	424	382	-10	-24	HMDB01372	1132	C00068
Trehalose	3.2	-	341	59	-80	-52	HMDB00975	1143	C01083
UDP-GlcNAc	8	-	606	159	-110	-66	HMDB00290	10705	C00043
Uridine 5'-monophosphate	7.9	-	323	79	-65	-66	HMDB00288	6030	C00105
Uridine 5-triphosphate (UTP)	8.6	-	483	159	-75	-45	HMDB00285	6133	C00075
Uridinediphosphate (UDP)	8.6	-	403	159	-90	-36	HMDB00295	6031	C00015
Uridinediphosphate-glucose	8.1	-	565	323	-85	-30	HMDB00286	439156	C00029

*** Internal standards**